WARSAW UNIVERSITY OF TECHNOLOGY Index 351733
FACULTY OF CIVIL ENGINEERING
COMMITTEE FOR CIVIL AND WATER ENGINEERING
POLISH ACADEMY OF SCIENCES ISSN 1230-2945

DOI: 10.24425/ace.2025.155089
ARCHIVES OF CIVIL ENGINEERING
Vol. LXXI ISSUE 3 2025
pp. 111 –128

Research paper

Structural and economic analysis of changes in design parameters of urban railway stations: a case study

Zhengyu Wu[1], Amirhossein Madadi[2], Mostafa Khoshtabkh[3], Seyed Mohammad Sajjadi-Attar[4], Behzad Nezamdoost[5], Basir Siami[6]

Abstract: Structural and economic analysis of changes in design and construction parameters of sections of urban railway stations is conducted. Station I2 of line 2 of Mashhad, Khorasan Razavi, Iran urban railway is considered as a sample station to be studied. Considering the existing condition of the station as a reference design, the effects of changes of concrete compressive strength, section height and type of rebar on load-bearing capacity of the structure are investigated. Further, economic analysis of the mentioned changes is conducted to obtain the most efficient design. The results indicate that bending members play more important roles; thus, an increase of concrete compressive strength could not substantially affect the decrease of area of reinforcement in those members. The minimum concrete compressive capacity that can be utilized in I2 station is C25 grade, so that the lower concrete grades could not meet the structural requirements. Furthermore, the results of parametrical analysis show that an increased concrete compressive strength as well as a decreased section height leads to a similar cost and load-bearing capacity to the reference design, while including better durability and lifetime characteristics. In this way, with the purpose of obtaining a similar load-bearing capacity to the reference design, utilization of rebar with increased strength grade (AIV instead of AIII rebar) can also result in decreasing the area of reinforcement, which can be followed by a 9% added value for the project.

Keywords: added value, parametrical analysis, P–M interaction, reinforce concrete, structural and economic analysis, urban railway (metro) station

[1] Associate Prof., PhD., School of Engineering, Fujian Jiangxia University, Fujian, Fuzhou 350108, China; Engineering Research Center of Phosphorus Resources Development and Utilization of Ministry of Education, Wuhan, Hubei 430000, China, e-mail: zhengyu_wu@fjjxu.edu.cn, ORCID: 0000-0001-5433-192X

[2] PhD. Student, Department of Civil and Environmental Engineering, Francis College of Engineering, University of Massachusetts Lowell, Lowell, MA 01854, USA; Director of Construction Materials Laboratory, The Thompson & Lichtner Co., Inc., Canton, MA 02021, USA, e-mail: amirhossein_madadi@uml.edu, ORCID: 0000-0002-9238-6507

[3] PhD. Student, Department of Civil Engineering, Neyshabur branch, Islamic Azad University, Neyshabur, Iran, e-mail: m.khoshtabkh@iau-neyshabur.ac.ir, ORCID: 0009-0003-2671-9953

[4] MSc., Eng., Department of Civil Engineering, Montazeri Technical College of Mashhad, Mashhad, Iran e-mail: sasajadi@tvu.ac.ir, ORCID: 0009-0009-9650-3430

[5] MSc. Student, Eng., Department of Civil Engineering, Hakim Sabzevari University, Sabzevar, Iran, e-mail: behzad.nezamdoost@gmail.com, ORCID: 0009-0000-7974-6638

[6] MSc., Eng., Department of Civil Engineering, Sharif University of Technology, Tehran, Iran, e-mail: basirsiami@gmail.com, ORCID: 0009-0000-8833-052X

1. Introduction

The growing demand for underground transportation systems in major cities requires constructing tunnels in urban areas, often in soft soil and shallow depths. This poses significant challenges for civil engineers in measuring, designing, and constructing these tunnels [1]. Analyzing tunneling-structure interaction is complex due to (i) interactions with adjacent structures, (ii) the three-dimensional nature of the problem, and (iii) nonlinear geometric behavior, necessitating advanced numerical methods [2].

Extensive research has focused on understanding the responses of tunneling-structure interactions, crucial for urban and interurban transportation networks. Recent literature abounds with analytical, numerical, and experimental studies addressing these complexities.

These observations, combined with the critical role of underground structures and tunnels in urban areas and interurban transportation networks, have driven extensive research on the tunneling-structure interaction response of embedded structures and tunnels. Numerous analytical, numerical, and experimental studies addressing these concerns are prevalent in recent literature.

Research on the stress state of composite linings is crucial for tunnel engineering design. Engineers use analogies and theoretical analyses to determine secondary lining parameters. Sauer et al. [3] used M-N curves to evaluate load-bearing capacity. Kasper et al. [4] examined the durability of steel fiber reinforced concrete (SFRC) linings. Qiu et al. [5] studied the effects of section dimensions and material strength through bending tests. Mai et al. [6] analyzed M-N curves of reinforced concrete columns, noting increased capacity with reduced reinforcement spacing. Ma et al. [7] employed finite difference methods to model tunnel-rock interaction and study fatigue in railway tunnels. Pengfei et al. [8] optimized tunnel construction schemes using 3D numerical simulations. Vanuvamal and Jaya [9] compared support designs, advocating for optimal shotcrete thickness, bolt specifications, and steel supports. Ghaffari and Mahdevari [10] simulated tunnel displacement under varying conditions. Many other researchers have also made significant contributions to tunnel engineering research with their findings and methodologies [11, 12].

Due to the expansion of urban railway lines in Iran and also following the objectives of Iran's 20-Year Vision Plan, access to concrete and concrete products with high strength as soon as possible and more economically is essential for this industry to be used in the development and construction of urban railway routes and stations [13, 14]. On the other hand, the economic evaluation of projects to reduce the cost of these products or, in other words, trying to achieve an efficient system is always one of the issues that attract the attention of everyone, especially project managers and officials, and play an important role in their major decisions [15, 16].

Analyzing parameters that affect the design of urban railway stations is crucial for sustainable development and reducing construction costs of concrete structures, especially in tunnels and urban train stations [17]. Additionally, economic evaluation based on design conditions, project implementation, and creating suitable conditions for decision-making are essential for selecting the best design and construction methods for such projects [18].

Accordingly, this study is conducted to evaluate the changes in the design parameters and construction of urban railway cross-sections structurally and economically and to investigate the use of affordable concrete in them. To this end, Station I2 of line 2 of Mashhad Urban Railway, Mashhad, Iran is studied as a sample. In this regard, changes in concrete strength grade, cross-section height, and type of rebar in one of the sections of the station are examined after the modeling and design of cross-sections. These changes are then evaluated economically to find the efficient design of cross-sections and calculate the added value.

2. Station I2

Mashhad Urban Railway project is the most important urban transportation system in Khorasan Razavi province. The main route of the project is Line 2, which is designed with an approximate length of 13;km from the end of North Tabarsi Boulevard to the south of Fazl Ibne Shazan Square. In this study, the modeling and calculations of the main structure of the central core of Station I2 are investigated. Station I2 is located between Stations H2 and J2 at the beginning of Koohsangi Street, south of Shariati Square (Taghiabad), and is the ninth station on this route. The axis of this station is located at 598.22 + 9 km of Line 2 of Mashhad Urban Railway. At the station, the average depth of the rail relative to the ground is about 20.7 m. The plan and location of Station I2 and the cross-sectional view of tunnel around this station can be seen in Fig. 1.

The geotechnical characteristics of the different layers of soil of I2 station obtained from geotechnical analysis report listed in Table 1.

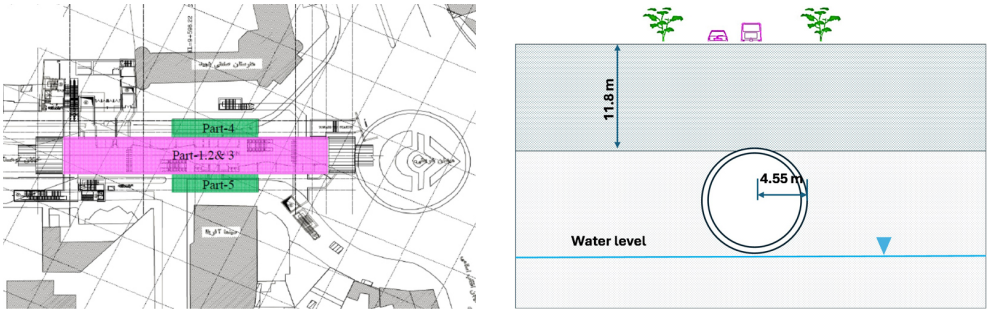

(a) (b)

Fig. 1. (a) Plan, and (b) schematic of the cross-sectional view of tunnel around the I2 Station

Table 1. Soil Characteristics

Layer	Desc.	E50 = Eoed (MPa)	E_{ur} (MPa)	φ	c (kN/m²)	Ψ	ν	K_0	γ_w (kN/m³)	ω
0-3m	Silty Clay	30	90	27	20	1	0.35	0.56	19	15%
3-6m	Sandy Clay	60	180	33	10	3	0.3	0.45	19	8-11%
6-9m	Silty Clay	35	105	27	25	1	0.35	0.56	19	15-20%
9-12m	Sandy Clay	80	240	33	10	3	0.3	0.45	19	6%
12-18m	Silty Clay	40	120	27	25	1	0.35	0.56	19.5	10-15%
18-20m	Sandy Clay	80	240	31	10	3	0.3	0.49	19.5	6-10%
20-32m	Silty Clay	30	90	22	20	1	0.35	0.61	20.5	14-21%
32-40m	Silty Clay	35	105	22	25	1	0.35	0.61	21	20-24%

The general cross-section of Station I2 is three stories. The schematic view of the station is shown in Fig. 2.

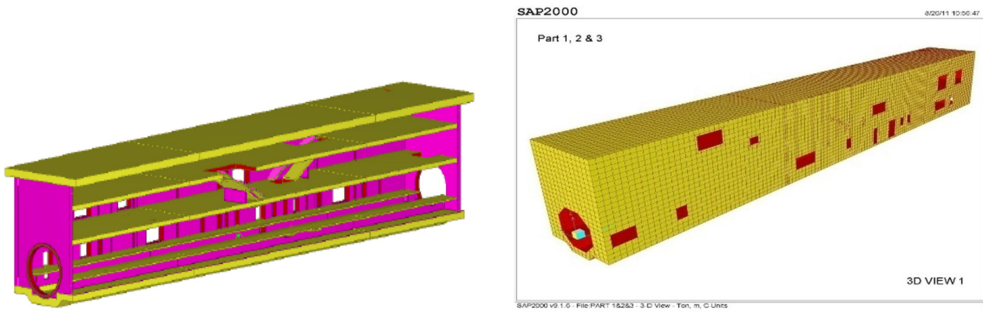

(a) (b)

Fig. 2. (a) Schematic view of the station, and (b) 3D view of the final model in SAP2000

3. Modelling and design parameters

The station's main structure was modeled using SAP2000 software based on detailed construction drawings (Fig. 2b). Walls and slabs were represented as shell elements with material characteristics from in-situ tests. Fixed supports were used at the raft level. With no visible damage, walls and slabs were modeled with gross section properties. Four-node shell elements represented all planar components, considering both membrane and plate-bending behaviors. Shell stiffness was determined using a four-point numerical integration method. Internal forces, moments, and stresses were calculated at 2-by-2 Gauss integration points and extrapolated to the joints in the local coordinate system. In the simulation model, the internal forces applied to the prefabricated parts are obtained using the force method and according to the effect of the joints of the concrete prefabricated parts, and in the parametrical analysis, the best combination of decision variables is sought to satisfy the geometrical, strength, and performance constraints of prefabricated concrete parts. Material specifications, geometrical properties of cross-sections, and loads are detailed in Tables 2 to 5 on software input specifications.

Table 2. Material specifications

Material	**Type**	**Design type**	**Unit mass (ton-s^2/m^4)**	**Unit weight (ton/m^3)**	***E*** **(ton/m^2)**	***U***
concrete	isotropic	concrete	2.5E-01	2.5E	2387500	0.2
rebar	uniaxial	rebar	8.0E-01	7.85E	21000000	0.0
steel	isotropic	steel	8.0E-01	7.85E	21000000	0.3

Table 3. Concrete design specifications

Material	F_c (ton/m2)	Rebar F_y (ton/m^2)	Rebar F_{ys} (ton/m^2)
concrete	2500	40000	40000

Table 4. Geometrical properties of cross-sections

Section	Material	Area type	Type text	Height (m)	M1, M11, and M22 modes
100–0.35	concrete	shell	Shell-thick	1.0	0.35
100–0.7	concrete	shell	Shell-thin	1.0	0.70
110–0.35	concrete	shell	Shell-thin	1.1	0.35
110v0.7	concrete	shell	Shell-thin	1.1	0.70
W18·35F	steel	shell	Shell-thin	0.0108	1.00
W18·35W	steel	shell	Shell-thin	0.00762	1.00

Table 5. Loads in modeling

Case	Load type	Load name	Load sf
Dead	Load case	Dead	1.00
SupDL	Load case	SupDL	1.00
LL	Load case	LL	1.00
LLT	Load case	LLT	1.00
SV	Load case	SV	1.00
SH	Load case	SH	1.00
SHcons	Load case	SHcons	1.00
EQ	Load case	EQ	1.00
EQVD	Load case	EQVD	1.00
PDELTA	Load case	Dead	1.00
PDELTA	Load case	SupDL	1.20
PDELTA	Load case	LL	1.20
PDELTA	Load case	LLT	1.60
PDELTA	Load case	SV	1.20
EQVT	Load case	EQVT	1.00

Static loads applied to the main structure are in different loading modes based on soil properties which are presented in Figs. 3 and 4. As seen, the loadings inlcude vertical loads caused by soil (SV), traffic (LLT), overhead dead (SupDL) and live load (LL); and

horizontal loads caused by laterals soil (SH) and surronding overhead (Shcons). The values of vertical loads are considered to be 4;t/m^2, 2;t/m^2, 0.3–0.4;t/m^2, 0.75–1.5;t/m^2 for SV, LLT, SupDL and LL, respectively, while for horizontal loads these values are 2.08–23.35;t/m^2 and 2.6;t/m^2 for SH and Shcons, respectively. Although seismic forces have a lesser impact on underground structures like tunnels and urban railway stations compared to above-ground structures, it is still crucial to control their design against ground motion during earthquakes. The effects of ground motion on underground structures fall into three categories: longitudinal bending, compression-extension, and ovalling/racking. Stresses from longitudinal bending and compression-extension are typically analyzed using a beam model in an elastic foundation, considering the environment as equivalent linear or nonlinear springs. These analyses are complex and have limited impact on the design, so construction joints are installed along the station to mitigate compression-extension [19].

Earthquake-induced distortion can be investigated using dynamic pressure, the free-field deformation method, and the soil-structure interaction (SSI) approach. This project uses the SSI method because it considers soil-lining interaction, tunnel excavation conditions, provides closed-form solutions for various cross-sections, incorporates the free-field deformation method, and uses peak ground acceleration at the construction site depth.

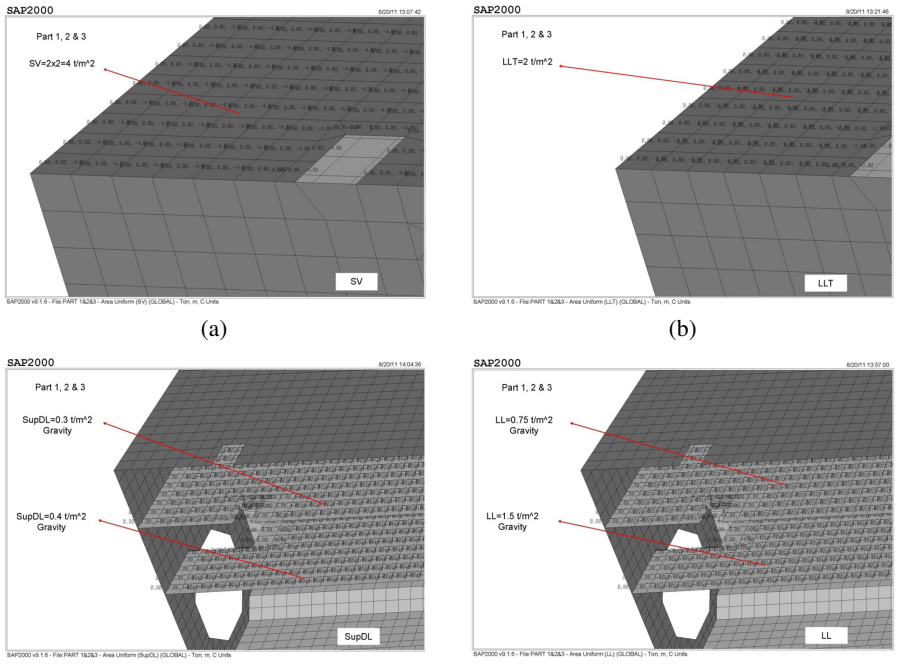

Fig. 3. Vertical loads caused by (a) soil (SV), (b) traffic (LLT), (c) dead overhead (SuperDL), and (d) live load (LL)

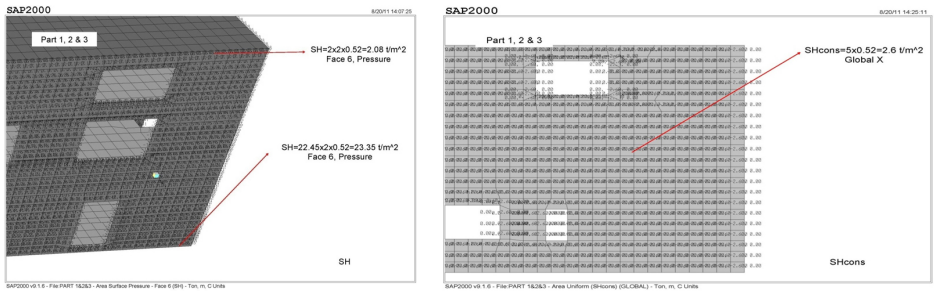

(a) (b)

Fig. 4. Horizontal loads caused by (a) lateral soil load (SH), and (b) lateral soil load due to surrounding overhead (SHcons)

The method of imposed displacement change is based on the response of a buried structure in soil. It determines soil mass rotation using specified soil seismic parameters. Considering the structure-to-soil stiffness ratio, it calculates the amplification coefficient of imposed rotation on the buried structure relative to the soil rotation mass. This displacement change is then applied to the structure based on a specific loading pattern.

3.1. The geodynamic parameters of the soil mass

The geodynamic parameters of the soil mass required for estimating the loads applied to the station are as follows:

1. Shear wave velocity (C_s): The value of C_s for the soil is determined based on geotechnical reports at each station location within the structure's placement range and is averaged.
2. Dynamic shear modulus of soil mass (G_m): G_m must also be determined from geotechnical studies. However, in the absence of this information, the dynamic shear modulus can be calculated using Eq. (3.1).

$$G_m = \rho \times C_s^2 \tag{3.1}$$

The value of C_s is determined as 725 m/sec based on weighted average of soil layers, and G_m is determined as 1051 MPa based on received soil reports and weighted average. The behavior of the soil mass around the station is assumed to be linearly elastic, and due to the dependence of the dynamic shear modulus on strain level and considering typical strains during earthquakes, the effective dynamic shear modulus of the soil (G_e) is considered as $G_e = 06G_m$. Therefore, G_e is calculated to be 630 MPa.

3. The maximum shear strain of the pristine soil mass ($\gamma_{\text{free-field}}$): $\gamma_{\text{free-field}}$, is given by Eq. (3.2).

$$\gamma_{\text{free-field}} = \frac{PGV}{C_s} \tag{3.2}$$

Here, PGV represents the maximum velocity of particle propagation within the station depth.

3.2. Seismic design parameters

The seismic parameter required for earthquake loading is the peak ground velocity (*PGV*) at the station depth. In seismic hazard studies, *PGV* can directly calculate $\gamma_{\text{free-field}}$. Alternatively, an approximate method can determine *PGV* at the station depth:

1. Determine *PGA* at station depth using soil profile acceleration graphs.
2. Identify desired station acceleration levels for 175 and 2000-year return periods from risk analysis, considering depth effects.
3. Calculate *PGV* from *PGA* considering station's distance from fault, soil type, and expected earthquake magnitude as per Table 2 in reference [20].

In the project's seismic risk analysis report, the design basis earthquake (target earthquake) is specified as 8.6 on the Richter scale, within a range of 3.6 to 3.7. However, given the Shandiz fault's seismic potential of up to 7.1 on the Richter scale within 20 kilometers of the project, a magnitude of 7.1 will be used to determine the ratio of wave propagation velocity to maximum earthquake acceleration for the entire project.

Therefore,

$$PGV = 122 \times PGA \text{ (for Stiff Soil \& SSD} = 0 - 20\,\text{km \& Mw} = 7.1) \tag{3.3}$$

Seismic Loading at Station The imposed deformation at the station is expressed as:

$$\gamma_{\text{structure}} = R \times \gamma_{\text{free-field}} \tag{3.4}$$

The coefficient R, which represents the ratio of the imposed deformation on the structure to the deformation in the soil environment, depends on the stiffness ratio between the structure and the soil and should be obtained from the displacement interaction method.

3.3. Closed-form solution

In this type of solution, the beam-on-elastic foundation approach is employed to model quasi-static soil-structure interaction effects, excluding dynamic (inertial) interaction effects. During seismic loading, the tunnel cross-section will undergo axial bending and shear strains resulting from free field axial, curvature, and shear deformations. The maximum axial strain, induced by a 45°incident shear wave is [20]:

$$\varepsilon_{\max^a} = 2\pi LA2 + E_1 A_c K_a 2\pi L^2 \leq fL4E_1 A_c \tag{3.5}$$

Where: L – wavelength of an ideal sinusoidal shear wave, K_a – longitudinal spring coefficient of the medium (in force per unit deformation per unit length of tunnel), A – free-field displacement response amplitude of an ideal sinusoidal shear wave, A_c – cross-sectional area of tunnel lining, E_l – elastic modulus of the tunnel lining, and f – ultimate friction force (per unit length) between the tunnel and surrounding soil.

The maximum frictional forces that can develop between the lining and the surrounding soils limit the axial strain in the lining. This maximum frictional force, $(Q_{\max})_f$, can be estimated

as the ultimate frictional force per unit length times one-quarter of the wavelength [21]. The maximum bending strain, resulting from a 0° incident shear wave is given by Eq. (3.6).

$$\varepsilon_{\max^b} = 2\pi L^2 A1 + E_1 I_c K_t 2\pi L^4 r \tag{3.6}$$

Where: I_c – the tunnel section's moment of inertia, K_t – transverse spring coefficient of the medium (force per unit deformation per unit length of tunnel), and r – half the height of a rectangular tunnel or radius of a circular tunnel.

Since both the liner and the surrounding medium are assumed to be linear elastic, their strains can be superimposed. Both positive and negative extremes must be considered as earthquake loading is cyclic. The maximum shear force on a tunnel cross-section, as a function of maximum bending strain, is given by Eq. (3.7).

$$V_{\max} = 2\pi L^3 E_1 I_c A_1 + E_1 I_c K_t 2\pi L^4 = 2\pi L M_{\max} = 2\pi L E_1 I_c \varepsilon_{\max} b_r \tag{3.7}$$

To estimate the total axial strain and stress conservatively, combine the strains from axial and bending forces as shown in Eq. (3.8).

$$\varepsilon^{ab} = \varepsilon_{\max^a} + \varepsilon_{\max^b} \tag{3.8}$$

These equations are crucial for structures in soft ground, while those in rock or stiff soils can be designed using free-field deformations. Notably, increasing the tunnel's stiffness and strength might attract more force rather than reduce it. A more flexible design with ductile reinforcement or flexible joints may be more effective [22].

4. Results and discussion

4.1. The effect of increasing the compressive strength of concrete

Different cross-sections are designed considering C25 concrete according to the capacity values of axial force, bending moment, and shear force in different parts of the station structure. In the following, axial force-bending moment (P–M) interaction diagrams for the wall cross-section are presented considering the design based on higher strength concretes (C30, C40, and C50) and comparison with the reference design (C25). Figure 5 shows the values of bending moment and axial force in a part of the wall as well as the designed cross-section (reference design) with a height of 1 m and a unit width for bending moment of 390 ton.m and axial force of 149 ton considering C25 concrete. The design of this cross-section, taking into account the increase in concrete capacity, can be seen in Fig. 6. Besides, the plus sign (+) in these figures indicates the coordinates of the desired point for the reference design (P = 149, M = 390). As can be seen, with increasing compressive strength of concrete, the compression capacity of the cross-section increases significantly, while its tensile capacity is not significantly changed [23].

Furthermore, for each of the 30, 40, and 50 MPa compressive strengths, analysis and design are performed again, and P–M interaction diagrams are drawn by reducing the number of rebars. Although this is done to provide the same interaction capacity as the reference design,

the results indicate that reducing the number of rebars has a greater effect on reducing the tensile capacity of the cross-section compared to its compressive capacity.

As can be seen in Fig. 6, the reduction of Rebar ∅32 to ∅28 in concrete grade C30 does not meet the structural requirements, while still providing the capacity required for the cross-section for grades C40 and C50. Reducing the same rebar to ∅25 does not meet the requirements

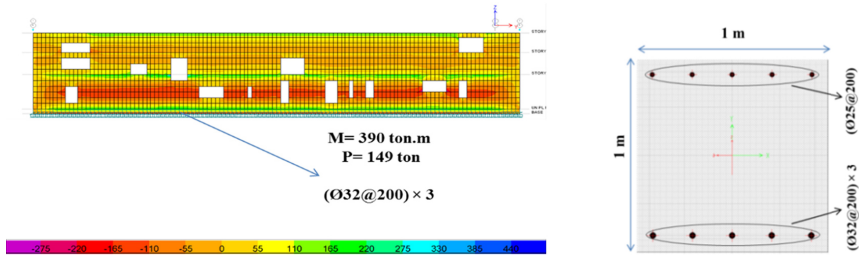

(a) (b)

Fig. 5. (a) The values of bending moment and axial force and (b) the designed cross-section wall with C25 concrete

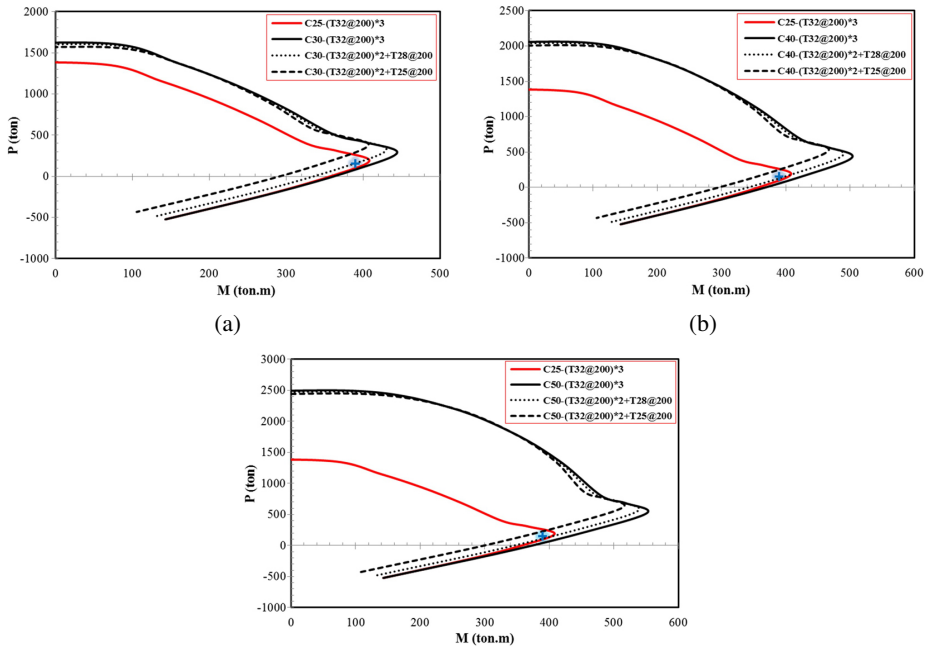

(a) (b)

(c)

Fig. 6. Axial force-bending moment interaction (P–M) in the wall cross-section for (a) C30, (b) C40, and (c) C50 concretes

in any of the concrete grades, and the cross-section does not have the bearing capacity of this amount of bending moment and axial force. However, it can be seen that increasing the concrete capacity does not significantly affect the tensile strength in the diagram. Although this increase in concrete grade leads to a reduction in rebar consumption, this decrease is not significant enough to cover the cost of increasing the concrete grade. In other words, no significant reduction can be observed in rebar consumption simply by considering the increase in the capacity of the cross-section due to the increase in concrete capacity. This can be attributed to the bending of the desired member (wall).

According to the results for the studied cross-section as a sample, it can be generally argued that most of the structural members of the urban railway station are bending and have bending performance. As a result, increasing the concrete capacity has no significant effect on increasing the ultimate moment capacity of the cross-sections. Increasing the capacity of concrete in members in which axial force is decisive can play a more effective role.

4.2. The effect of reducing the compression capacity of concrete

The *P–M* diagrams for the strength grade lower than C25 with a fixed design for all of them are shown in Fig. 7. As seen, for the desired point, the reduction of concrete capacity does not meet the capacity of the axial force required at this point. So, the minimum concrete grade that can be used is C25.

4.3. The effect of changes in the height of cross-sections

Another factor affecting the bearing capacity and *P–M* interaction diagrams of cross-sections is the change in their height considering different concrete capacities. Figure 8 shows *P–M* interaction diagrams to investigate the effect of changes in the height of cross-sections at different concrete grades. As seen, the red diagram (continuous line) belongs to the initial design of the wall cross-section with concrete grade C25. At concrete grade C25, reducing the

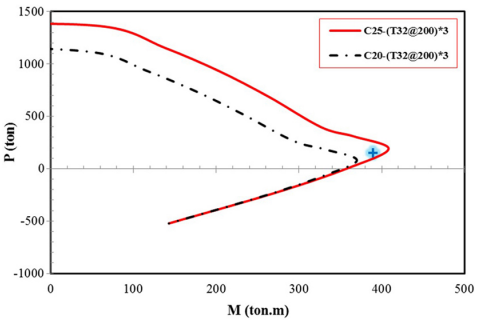

Fig. 7. Effect of reduction of concrete compression capacity on axial force-bending moment (*P–M*) interaction in the wall cross-section

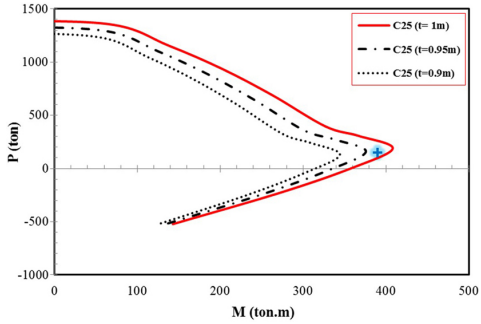

Fig. 8. Effect of reducing the height of the cross-section on axial force-flexural moment (*P–M*) interaction in the wall cross-section for C25 concrete

height of the cross-sections from 1 m to 0.95 m leads to a decrease in their capacity so that the created capacity does not meet the requirements of the cross-sections. So, at this concrete grade, reducing the height of the cross-sections is not justified.

At the strength grades of concrete C30, C40, and C50, the effect of change in the height of the cross-section is investigated, the results of which are provided in Fig. 9. In this analysis, the initial design (continuous red diagram) is considered as the reference design, and the height of the cross-section is reduced to the extent that the cross-section designed with higher-grade concrete satisfies the axial force and the bending moment of the initial cross-section. As seen, by reducing the height of the cross-section to 0.95 m, the tensile capacity of the cross-section (especially for concrete grades C40 and C50) continues to meet the requirements of the cross-section (initial design) using higher strength concrete. However, reducing the height to 0.9 m leads to a lower capacity than the initial design. On the other hand, increasing concrete strength grade causes a significant increase in the compression capacity of the cross-section but does not change the tensile capacity of the cross-section significantly.

As seen in Fig. 9(a), given that the desired point (plus sign) is approximately on the diagram of concrete grade C30 and the height of 0.95 m for the cross-section, it can be argued that height of 0.95 m for the cross-section and concrete grade C30 can still meet the required capacity of

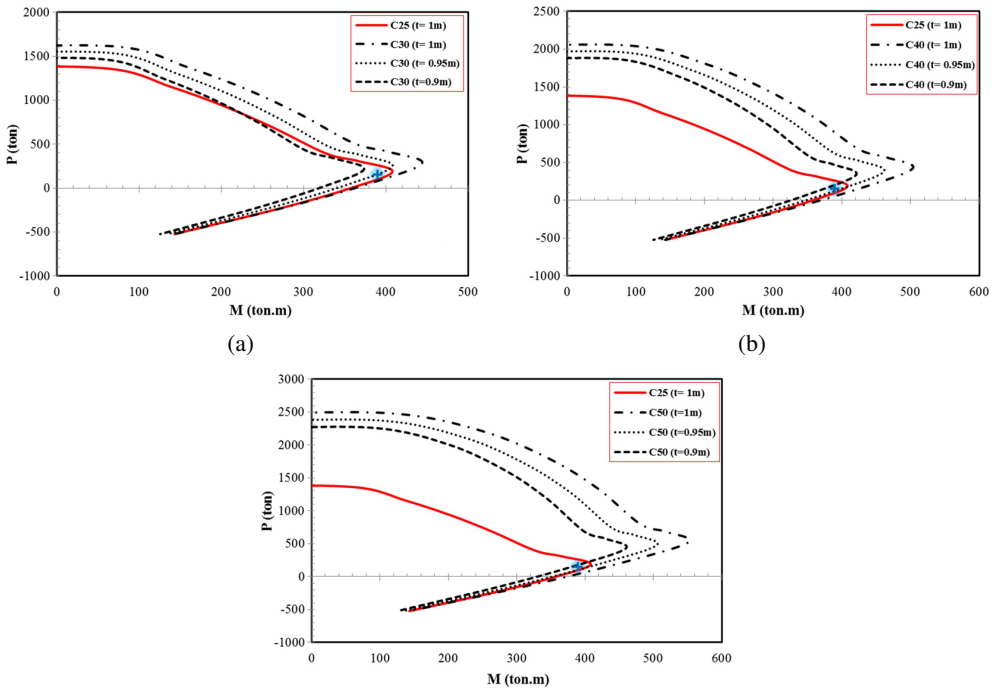

Fig. 9. The effect of reducing the height of the cross-section on axial force-bending moment (P–M) interaction in the wall cross-section for (a) C30, (b) C40, and (c) C50 concrete grades

the cross-section and be considered as the efficient design for this section (considering the initial design as the reference design). Accordingly, the cost of this design (concrete C30 grade and height 0.95 m) is estimated to be compared with the original design (concrete grade C25 and height of 1 m) in this cross-section (the prices are based on those approved by the Concrete Association of Khorasan Razavi, dated April 06, 2021):

The reduction of concrete consumption due to the reduction of height from 1 m to 0.95 m:

$$\frac{1\,(\mathrm{m}) - 0.95(\mathrm{m})}{1(\mathrm{m})} \times 100 = 5\% \tag{4.1}$$

The increase in concrete prices due to the increase in concrete grade from C25 to C30:

$$\frac{5520000(\mathrm{C30}) - 5270000(\mathrm{C25})}{5520000} \times 100 \simeq 4.5\% \tag{4.2}$$

As seen, using the design with concrete C30 grade and height of 0.95 m has 0.5% added value rather than the design with concrete grade C25 and height of 1 m. However, higher concrete grade (C30 instead of C25) with a reduced height of the cross-section can be used as the efficient design because higher concrete grade can provide better durability and lifetime for the structure [24]. The use of concrete with a strength grade higher than C30 (C40 or C50) cannot be justified because the increase in price due to the production of this type of concrete is more than the reduction in cost due to reduced height of the cross-section.

4.4. The effect of changing the type of rebar

Since type AIII rebar (yield stress of 400 MPa (S400)) is used in the Station I2 structure and the production of concrete parts, this study examines rebars AII (yield stress of 340 MPa (S340)) and AIV (yield stress of 500 MPa (S500)) and the effect of their application on the design of the cross-section. Figure 10 shows the effect of rebars S340 and S500 on the P–M interaction of the wall cross-section. As seen, reducing the strength of the rebar (at concrete grade C25) reduces the tensile capacity of the cross-section and, consequently, does not meet the required capacity requirements, taking into account the continuous red line as the initial design and acceptable default conditions. On the other hand, increasing the strength capacity of concrete does not significantly affect the increase in the tensile capacity of the cross-section and cannot play an important role in compensating for the decrease in capacity caused by the reduction of rebar strength.

According to Fig. 10(b), which shows the design of the cross-section with rebar S500 and concrete grade C25, increasing the rebar strength increases the tensile capacity of the cross-section. All diagrams are designed with concrete grade C25 because increasing the strength grade of concrete does not have a significant effect on the tensile capacity of the cross-section. Therefore, the requirements of the cross-section in these conditions are changes in its tensile capacity. Since the design with concrete grade C25 also meets the compressive capacity required for the section, there is no need to increase the concrete grade. On the other hand, the results show that fewer number of rebar S500 can be used than rebar S400 to provide the desired capacity (i.e. initial design). As seen, the number of rebars can be reduced until

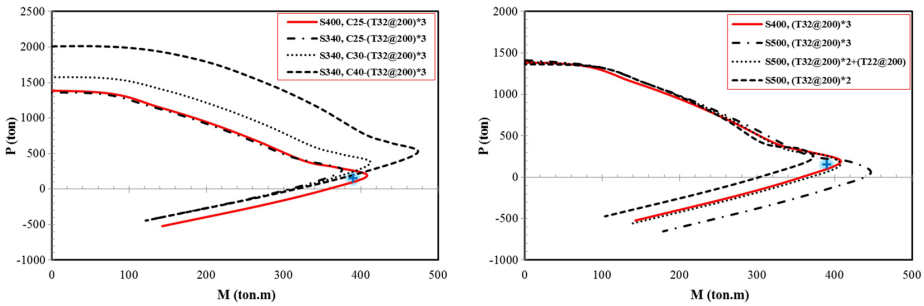

(a) (b)

Fig. 10. The effect of (a) reducing and (b) increasing the rebar strength on axial force-bending moment (P–M) interaction in the wall cross-section

the initial design is achieved (continuous red diagram) by using AIV type rebars so that two ∅32 and one ∅22 can be used instead of three ∅32, and the desired axial force and bending moment can be provided. It can be seen in Fig. 10(b) that the P–M interaction diagrams of these two designs are most consistent with each other.

These two types of design are compared economically as follows:

The reduction of rebar consumption due to the use of two ∅32 and one ∅22 of type AIV instead of three ∅32 of type AIII:

$$1) \quad (\varnothing 32@200) \times 3 = 120.6 \text{ cm}^2 \tag{4.3}$$

$$2) \quad (\varnothing 32@200) \times 2 + (\varnothing 22@200) = 99.4 \text{ cm}^2 \tag{4.4}$$

$$\rightarrow \frac{120.6 - 99.4}{120.6} \times 100 \simeq 18\%$$

The price increase is about 9% due to the change in the type of rebar from S400 to S500. So, reducing the cost of rebar consumption is as follows:

$$18\% - 9\% = 9\% \tag{4.5}$$

Considering the cost reduction rate in the station walls, the rate of cost reduction according to the number of longitudinal rebars of the cross-sections of the wall in Station I2, taking into account the rebar price, which is about 230000 Rials per kilogram, is as follows:

The share of longitudinal rebars of the wall from the total rebars used in the station:

$$0.43 \text{ (wall/total)} \times 0.7\text{(lon/tran)} = 0.3 \tag{4.6}$$

$$1787000 \text{ (kg)} \times 0.3 \times 230000 \text{ (Rials)} \times (9\%) \simeq 11,100,000,000 \text{ Rials} \tag{4.7}$$

4.5. The simultaneous effect of parameters

According to the results obtained in the study of the effect of different design parameters, the simultaneous effect of increasing the concrete and rebar grade and reducing the height of the cross-section on the interaction of axial force-bending moment (P–M) of the wall

cross-section is investigated, the results of which are provided in Fig. 11. As can be seen, Design I includes the use of concrete grade C30, a height of the cross-section of 0.95 m, and two ∅32 and one ∅22 of type AIV rebar instead of three ∅32 of type AIII rebar. In evaluating the effect of changing the parameters individually, the results show that increasing the concrete grade and decreasing the height of the cross-section cause an almost a break-even point and that the use of higher-grade rebar brings a total of 9% added value. As a result, the design could have a total value of 9%.

According to Fig. 11, Design II, which has a shorter height of cross-section and more rebars than Design I, does not meet structural requirements and has a lower capacity than expected. So, it is excluded from the evaluations.

However, it can be seen that Design III, which includes the use of concrete grade C35, a height of the cross-section 0.9 m, and two ∅32 and one ∅25 of type AIV rebar instead of three ∅32 of type AIII rebar, has the capacity required for the structure. The following is an economic evaluation of Design III compared to the reference design.

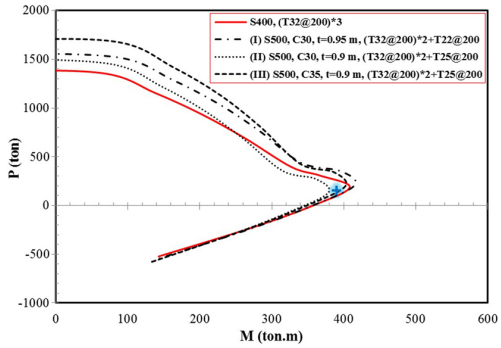

Fig. 11. The simultaneous effect of changing design parameters on axial force-bending moment (P–M) interaction in the wall cross-section

The rate of reduction of concrete consumption due to the reduction of height from 1 m to 0.9 m:

$$\frac{1(\mathrm{m}) - 0.9(\mathrm{m})}{1(\mathrm{m})} \times 100 = 10\% \tag{4.8}$$

The rate of increase in concrete prices due to the increase in concrete grade from C25 to C35 (the prices are based on those approved by the Concrete Association of Khorasan Razavi, dated April 06, 2021):

$$\frac{5770000(\mathrm{C35}) - 5270000(\mathrm{C25})}{5770000} \times 100 \simeq 8.7\% \tag{4.9}$$

The rate of reduction in rebar consumption due to the use of two ∅32 and one ∅25 of type AIV rebar instead of three ∅32 of type AIII rebar:

$$1) \quad (\varnothing 32@200) \times 3 = 120.6\mathrm{cm}^2 \tag{4.10}$$

(4.11) 2) $(\varnothing 32@200) \times 3 + (\varnothing 25@200) = 104.9\,\text{cm}^2$

(4.12) $$\rightarrow \frac{120.6 - 104.9}{120.6} \times 100 \simeq 13\%$$

The rate of increase in price due to the change in the type of rebar from S400 to S500 is about 9%. For the total increase and decrease of prices we have:

(4.13) $$13\% - 9\% + 10\% - 8.7\% = 5.3\%$$

As can be seen, the use of Design III brings 5.3% added value compared to the reference design. By comparing Designs I and III, it is found that Design I with 9% added value is a better design than design III with 5.3% added value. However, thanks to the use of concrete grade C35 in Design III, this design can also be used in cases where higher durability and strength of concrete are required and provide better lifetime for the structure.

According to these evaluations, change in any of the effective parameters can play a decisive role in the design of cross-sections and, consequently, the final cost of the structure. However, the implementation of these parametrical analyses to reduce the costs depends on the conditions and requirements of the construction.

5. Conclusions

The main findings of this study are as follows:

1. Most of the structural members of the urban railway station are flexural elements and have bending performance. As a result, increasing the concrete compressive strength has no significant effect on increasing the ultimate moment capacity of the cross-sections. Increasing the capacity of concrete in members in which axial force is decisive can play a more effective role. In other words, no significant reduction can be observed in rebar consumption simply by considering the increase in the capacity of the cross-section due to the increase in concrete grade.
2. According to the analysis of the effect of reducing the compression capacity of concrete, the minimum concrete strength grade that can be used for reinforced concrete buildings is C25, and lower strength grades do not meet the requirements for capacity of the axial force.
3. The evaluation of effect of changes in the height of cross-sections indicates that the use of higher-grade concretes in cross-sections with reduced height can provide the required capacity with the same cost as lower-grade concretes with higher height of the cross-section. For instance, the price of C30 grade concrete with height of cross-section = 0.95 m is similar to that of C25 grade concrete with height of cross-section = 1 m. Therefore, utilizing higher-grade concretes can be more beneficial as it provides improvement of durability and lifetime of the structure.
4. The analysis of the effect of changing the type of rebar indicates that the use of higher strength rebar with less amount can meet the structural design requirements, and at the same time effectively reduces the cost of design. For instance, in a similar cross-section

and concrete grade, type AIV (S500) rebars can be used with fewer amount compared to type AIII (S400) rebars to achieve a cost reduction of about 9%.

5. The investigation of simultaneous effect of parameters indicates that the combination of different values of each design variables (i.e. concrete grade, cross-section geometry, type of rebar, etc) can be alternatively applied into the design procedures to help us obtain the most efficient and cost-effective values.

Acknowledgements

This research is supported by financial grants from "the National Natural Science Foundation of China (52104122)", "the Open Project of Engineering Research Center of Phosphorus Resources Development and Utilization of Ministry of Education (LKF2021007)", and "the Natural fund project of Fujian Province Science and Technology Department (2020J0212307)".

References

[1] H. Liu, J.C. Small, and J.P. Carter, "Full 3D modelling for effects of tunnelling on existing support systems in the Sydney region", *Tunnelling and Underground Space Technology*, vol. 23, no. 4, pp. 399–420, 2008, doi: 10.1016/j.tust.2007.06.009.

[2] H. Mroueh and I. Shahrour, "A full 3-D finite element analysis of tunneling–adjacent structures interaction", *Computers and Geotechnics*, vol. 30, no. 3, pp. 245–253, 2003, doi: 10.1016/S0266-352X(02)00047-2.

[3] G. Sauer, V. Gall, E. Bauer, and P. Dietmaier, "Design of tunnel concrete linings using capacity limit curves", in *Proceedings of the Eighth International Conference on Computer Methods and Advances in Geomechanics*, 1994.

[4] T. Kasper, C. Edvardsen, G. Wittneben, and D. Neumann, "Lining design for the district heating tunnel in Copenhagen with steel fibre reinforced concrete segments", *Tunnelling and Underground Space Technology*, vol. 23, no. 5, pp. 574–587, 2008, doi: 10.1016/j.tust.2007.11.001.

[5] Y. Qiu, K. Feng, C. He, L. Zhang, and C. Wang, "Investigation of the ultimate bearing capacity of a staggered assembly segmental lining for an urban gas transmission tunnel", *Sustainable Cities and Society*, vol. 48, art. no. 101551, 2019, doi:10.1016/j.scs.2019.101551.

[6] A.D. Mai, M.N. Sheikh, and M.N. Hadi, "Failure envelopes of square and circularized RC columns discretely confined with CFRP", *Construction and Building Materials,* vol. 261, art. no. 119937, 2020, doi: 10.1016/j.conbuildmat.2020.119937.

[7] W. Ma, et al., "Research on Design Parameters and Fatigue Life of Tunnel Bottom Structure of Single-Track Ballasted Heavy-Haul Railway Tunnel with 40-Ton Axle Load", *Mathematical Problems in Engineering,* vol. 2020, art. no. 3181480, 2020, doi: 10.1155/2020/3181480.

[8] J. Pengfei, X. Zhang, X. Li, B. Jiang, B. Liu, and H. Zhang, "Optimization analysis of construction scheme for large-span highway tunnel under complex conditions", *Archives of Civil Engineering*, vol. 64, no. 4/I, pp. 55–68, 2018.

[9] A. Vanuvamalai and K. Jaya, "Design analysis of an underground tunnel in Tamilnadu", *Archives of Civil Engineering*, vol. 64, no. 1, pp. 21–39, 2018, doi: 10.2478/ace-2018-0002.

[10] M. Ghaffari and S. Mahdevari, "The effect of tunnel geometry and geomechanical parameters of host rock on tunnel displacement profile", *Geotechnical and Geological Engineering*, vol. 40, no. 5, pp. 2799–2809, 2022, doi: 10.1007/s10706-022-02063-3.

[11] J. Zhang and Y. Qi, "Research on the intelligent positioning method of tunnel excavation face", *Archives of Civil Engineering*, vol. 68, no. 1, pp. 431–441, 2022, doi: 10.24425/ace.2022.140178.

[12] W. Han, T. Xiao, D. Shi, and Y. Wang, "Optimization of heavy haul railway tunnel lining based on ultimate bearing capacity", *Archives of Civil Engineering*, vol. 68, no. 4, pp. 493–511, 2022, doi: 10.24425/ace.2022.143051.

[13] H. Eskandari and A. Madadi, "Investigation of ferrocement channels using experimental and finite element analysis", *Engineering Science and Technology, an International Journal*, vol. 18, no. 4, pp. 769–775, 2015, doi: 10.1016/j.jestch.2015.05.008.

[14] A. Madadi, H. Eskandari-Naddaf, and M. Gharouni-Nik, "Lightweight Ferrocement Matrix Compressive Behavior: Experiments Versus Finite Element Analysis", *Arabian Journal for Science and Engineering*, vol. 42, no. 9, pp. -4001–4013, 2017, doi: 10.1007/s13369-017-2557-4.

[15] P. Ghoddousi, E. Eshtehardian, S. Jooybanpour, and A. Javanmardi, "Multi-mode resource-constrained discrete time–cost-resource optimization in project scheduling using non-dominated sorting genetic algorithm", *Automation in Construction*, vol. 30, pp. 216–227, 2013, doi: 10.1016/j.autcon.2012.11.014.

[16] T. Korouzhdeh, H. Eskandari-Naddaf, and M. Gharouni-Nik, "An Improved Ant Colony Model for Cost Optimization of Composite Beams", *Applied Artificial Intelligence*, vol. 31, no. 1, pp. 44–63, 2017.

[17] A. Madadi, M. Tasdighi, and H. Eskandari-Naddaf, "Structural response of ferrocement panels incorporating lightweight expanded clay and perlite aggregates: Experimental, theoretical and statistical analysis", *Engineering Structures*, vol. 188, pp. 382–393, 2019, doi: 10.1016/j.engstruct.2019.03.038.

[18] M. Shariat, M. Shariati, A. Madadi, and K. Wakil, "Computational Lagrangian Multiplier Method by using for optimization and sensitivity analysis of rectangular reinforced concrete beams", *Steel and Composite Structures*, vol. 29, no. 2, pp. 243–256, 2018, doi: 10.12989/scs.2018.29.2.243.

[19] S. Abbas, "Structural and durability performance of precast segmental tunnel linings", PhD. thesis, University of Western Ontario, Canada, 2014.

[20] Y.M. Hashash, J.J. Hook, B. Schmidt, I. John, and C. Yao, "Seismic design and analysis of underground structures", *Tunnelling and Underground Space Technology*, vol. 16, no. 4, pp. 247–293, 2001, doi: 10.1016/S0886-7798(01)00051-7.

[21] A. Sakurai and T. Takahashi, "Dynamic stresses of underground pipelines during earthquakes", in *Proceedings 4th World Conference on Earthquake Engineering*. 1969, pp. 81–95.

[22] J. Wang, *Seismic design of tunnels: a state-of-the-art approach*. New York: Parsons, Brinckerhoff Inc., 1993.

[23] A. Madadi, H. Eskandari-Naddaf, and M. Nemati Nejad, "Evaluation of bond strength of reinforcement in concrete containing fibers, micro-silica and nano-silica", *Journal of Stress Analysis*, vol. 3, no. 1, pp. 11–19, 2018, doi: 10.22084/jrstan.2018.15436.1036.

[24] A. Madadi, H. Eskandari-Naddaf, R. Shadnia, and L. Zhang, "Digital image correlation to characterize the flexural behavior of lightweight ferrocement slab panels", *Construction and Building Materials*, vol. 189, pp. 967–977, 2018, doi: 10.1016/j.conbuildmat.2018.09.079.

Received: 2024-03-17, Revised: 2024-07-03